Towards realistic 3D elastic models of Canadian channel and reef structures

Gary F. Margrave, Samantha Taylor, and Joanna K. Cooper

ABSTRACT

We discuss the creation of two detailed elastic models of Canadian stratigraphic exploration targets and present initial views of wavefield simulations through these targets. Our first model, which is a buried channel sequence beneath a stratified overburden, is more mature than our second model, which is a pinnacle reef beneath a stratified over burden. The process used to create both models was similar. We began by creating geologically plausible maps at five depth levels within the channel system or the reef. The maps were intended to be similar, but not identical, to known structures. Seven distinct lithologies were identified for each model and these maps specified polygonal regions, which were each assigned one of the lithologies. The maps were then digitized and, for each map, three duplicates were created specifying Vp, Vs, and density as uniform properties within 2D polygons. Then a specially developed 3D kriging algorithm was used to interpolate a number of new maps between each digitized one. This process also created plausible property gradients within the polygons on the original maps. The resulting channel structure contains 13 levels each described by a 241x241 grid while the reef structure contains 24 levels on a somewhat larger grid. An overburden and underlying succession, which vary only vertically, were then crafted for each model from smoothed representations of available well logs. The final 3D models specify Vp, Vs, and density at all points in the 3D volume. The channel sequence is 120m thick at a depth of 1 km and with horizontal apertures of 2.7km in each direction. The reef model is slightly larger and deeper. Sample 3D shots have been simulated at several positions over the channel model using our Rayleigh-Sommerfeld algorithm and using a commercial finite-difference code. The simulations show that our models produce a very complex elastic response that can be used to evaluate the performance of imaging algorithms and to study footprint effects.

INTRODUCTION

Seismic modelling is an essential tool in the seismic exploration process. In simple terms, the process requires the specification of an earth model and the subsequent calculation of its seismic response. Earth models are prescriptions of earth properties that are relevant to seismic wave propagation as a function of position in the subsurface. They can range from very simple homogeneous media to complex environments comparable to those actually found in the earth. Models can be specified in 1, 2, or 3D and, even though our world is fully 3D, the reduced dimensional models are extremely useful. Often 1D models are created from well log measurements and can describe an extremely detailed stratigraphy. Synthetic seismograms computed from such 1D models are the most common modelling product, whose primary use is to correlate observed seismic events on migrated sections with well log information. Higher dimensional models are usually used to test data processing and imaging methods and can be used to demonstrate whether or not subtle features are actually observable. Often 2D and 3D models consist of homogeneous blocks of material without the fine stratigraphic seen in

well logs. Such idealized constructions can answer many questions but it is becoming more and more common to define a great deal of stratigraphic and structural detail as in seen in the Marmousi model or the SEG/EAGE series of models. Our goal here is to construct detailed models representing typical, but not specific, Canadian stratigraphic exploration targets such as channels and reefs. In this paper we present our initial results and solicit suggestions for improvement.

The second phase of modelling, that of calculating the seismic response, is technically complex and requires a number of decisions, often involving compromises between what is realistic and what is computable. No geophysicist would dispute the assertion that the earth is better approximated as a 3D elastic medium, complete with heterogeneity and anisotropy, than as a 3D acoustic medium in which only pressure waves can propagate. Even so, 3D and even 2D acoustic models have tremendous value, and much effort has been expended in their construction and in the analysis of the predicted seismic response. The utility of acoustic models comes from perhaps the central compromise of production land seismic exploration and that is the recording of only the vertical component of ground motion, subsequently, the assumption is that only compressional waves have been collected and that the wavefield is scalar-valued. This facilitates the current generation of seismic imaging algorithms that can handle very complex environments and large datasets but assume scalar waves. Of course, seismic waves are vector-valued and CREWES has been one of a few groups pushing the incorporation of 3C data and vector algorithms into the seismic method. While there is still a great deal about 3D elastic wave propagation that is not well understood, enough is known to attempt construction of limited classes of 3D elastic models. Here we report on 3D elastic models for stratigraphic, not structural, environments.

Most Canadian oil and gas production comes from fields in the Western Canadian Sedimentary Basin where the plays are dominated by stratigraphic considerations. Realistic 3D models for complex, yet non-specific settings, such as buried channels, pinnacle or platform reefs, or similar structures would have many uses. Seismic responses from such models would be valuable as training datasets for students of data processing and imaging. Experienced researchers would find them useful to test imaging algorithms and inversion techniques. Explorationists could use the seismic responses to ask and answer questions such as "Does my acquisition geometry bias the observed AVO?" or "How reliably can the AVO from very small sand bodies be measured?" Even management and HR groups might find the resulting images useful as recruiting devices.

Previously (Margrave and Cooper, 2007), we have reported on our initial development of 3D modelling by direct implementation of the Rayleigh-Sommerfeld theory of diffraction. Using this method, we were able to construct a 3D scalar-wave dataset that we termed "exhaustive" because it had a sufficient density of sources and receivers such that neither source gathers nor receiver gathers had any spatial aliasing. Elsewhere in this report (Cooper and Margrave, 2008) we describe the extension of the Rayleigh-Sommerfeld method to scalar-waves with P-P elastic AVO. This is a first step towards full elastic modelling with Rayleigh-Sommerfeld which we intend to explore in the coming year. In this paper we will show initial calculations of seismic responses from our elastic models using both the Rayleigh-Sommerfeld approximation and a full 3D elastic

finite-difference method, the Tiger code by SINTEF Petroleum Research[1] of Trondheim, Norway.

The construction of our models was influenced by a number of considerations. We wanted to keep the models small enough that construction of exhaustive datasets was not completely impossible, which implies a linear aperture of less than about 3km. This in turn means that our target structures should not be deeper than about 1.5km. Also, we desired stratigraphically complex targets but the overburden was kept to a simple horizontally layered medium. We chose to model a buried channel system and a pinnacle reef but we did not want these to be actual models of real structures. So we used real structures as a guide but also varied them in significant, sometimes arbitrary, ways. For example, we used surface maps of the present-day Bow River as our channel model and took published rock properties values from work done on the Glauconitic Channel systems in southeast Alberta.

In the next section, we describe the process of constructing our channel model, and in the subsequent section we show some preliminary seismic responses. Then, in a final section, we show images of our reef model.

THE CREWES CHANNEL AND REEF MODELS

Channel Model

When building this complex 3D model, it was imperative that we started with a system that was not only believable from a geologic perspective, but also a valid example of meandering rivers that are seen locally in Alberta. To accomplish this, a modern but mature river system was paired with data and lithologies obtained from logs on similar river systems at depth. The Bow River was chosen as the modern muse due to its locality, as well as for the abundance of aerial maps in the public domain. This allowed for the precise selection of an interesting area along the channel. It was also necessary for this model that the aerial view was at a very small scale of only a few kilometres at the most, any larger, and it would be difficult to distinguish fine fluctuations in lithology that were desired in the model. As for the data, these were selected from a number of sonic logs throughout the Blackfoot-Cavalier field in Southern Alberta, which contains glauconitic channel sands at a depth which is appropriate for the size and depth of this model.

To properly distribute differing channel lithologies through 3D space, over the span of thousands of years, the movement of the river back through time had to be taken into account. Thus, based on the modern image of the Bow River that was originally chosen, a series of maps representing past surfaces had to be envisioned so that the river appeared to move fluidly through the area. For each increment taken backwards in time, every bend and curve in the river was moved upstream to migrate different lithology bodies to potential past locations. In the Bow River area, easily discernable examples of such previous levels are not preserved, as the river has not always been an aggrading system. After an initial post-glacial incision, the river experienced around 6,000 years of aggradation (Hills, 2002) carrying a heavy bed-load of till material, and has since been incising into modern times. Combining this discontinuous time frame with the fact that

---

[1] *www.**sintef**.no/upload/Petroleumsforskning/Brosjyrer/**TIGER**.pdf*

the Calgary area is riddled with till bodies (Osborn and Rajewicz, 1998), the projected slices of the past Bow River are necessarily fictional, and have been produced with detailed research of the area, geological foresight, and a little artistic license. They are not in any way a representation of what the Bow River itself actually looked like, as this is not truly known. The modern Bow River was simply a starting point on which to create a generic aggrading river system that was in a local setting, of similar size, and had experienced the same sort of geological history as many river systems throughout Alberta.

Initial Maps and Overburden
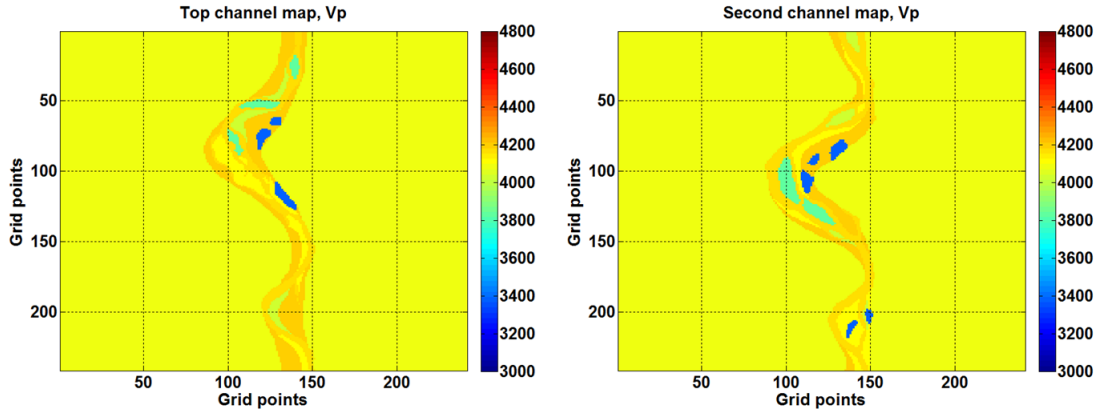
FIG. 1. Images of the modern Bow River (left) and the projection of the deposited channel lithologies at a depth of 30m below present ground surface (right). The colour scale shows values of P-wave velocity in m/s.

Figure 1 shows the digitized map of the actual Bow river and its first hypothesized antecedent. A total of five such maps were produced. Digitization was done on a 241x241 grid. Polygonal regions were defined in the digitizing and each polygonal region was initially assigned a homogeneous lithology. Based on general sand types that are typical in a river system, seven different lithologies were assigned: poor quality sand (1), moderate quality sand (2), good quality sand (3), very good quality sand (4), channel (a non-prospective sand) (5), sandy shale (6), and regional material (7). Each lithology assignment then implies a particular P-wave velocity, S-wave velocity, and density. Values for these parameters (Table 1) were based on the data from sonic and density logs taken within the Blackfoot-Cavalier field near Strathmore, Alberta (Potter et al., 1996), and are representative of the Glauconitic channel system.

Table 1. Data used in Bow River lithology assignments, based on sonic logs from Glauconitic incised valleys

	Poor sand	Moderate sand	Good sand	Very good sand	Channel	Sandy Shale	Regional Material
Vp (m/s)	4200	4110	4035	3820	4160	3380	4095
Vs (m/s)	2135	2180	2275	2310	2240	1610	2048
Rho (kg/m^3)	2560	2530	2475	2420	2545	2600	2500
Vp/Vs	1.97	1.89	1.77	1.65	1.86	2.10	2.00

The Glauconitic channel system occurs at a depth of roughly 1.5 km at the Blackfoot-Cavalier field. In order to control the final model size while still ensuring a good range of seismic incidence angles we eventually choose to place our hypothetical channel system at a depth of 1km. The overburden (Figure 2) was modelled by smoothing the available log information and assuming a constant Vp/Vs of about 2.1 except for the first 500m where this value was allowed to gradually approach 3.0. Changing the depth of the channel system was reflected in the lithology properties by rescaling them using the scale factor property_value(1000m)/property_value(1500m). Scale factors were 0.864 for Vp, 0.871 for Vs, and 0.928 for density. Figure 3 recreates Figure 1 but with the Vp values rescaled and the colour bar adjusted. Figure 4 is similar except that the value of Vp/Vs is shown; potential exploration targets are presumed to have low values of this ratio.
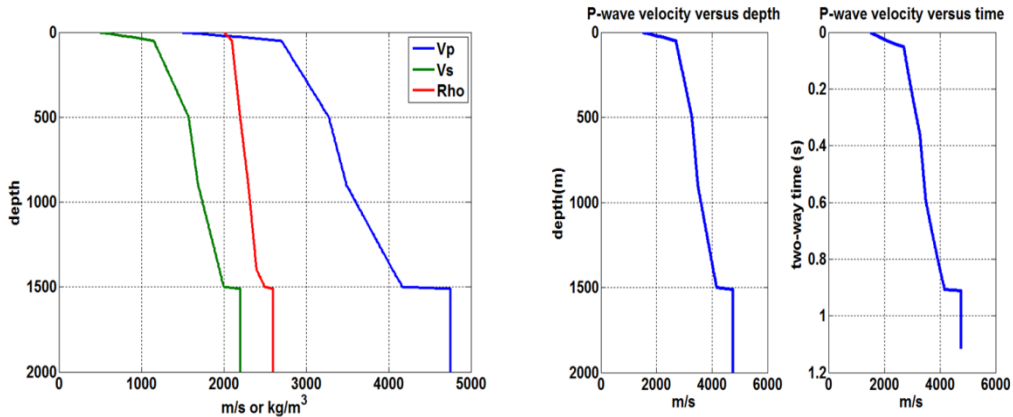
FIG. 2. (Left) The background model as implied by smoothing available well information. (Right) The background Vp displayed in both depth and 2-way P-wave vertical traveltime.
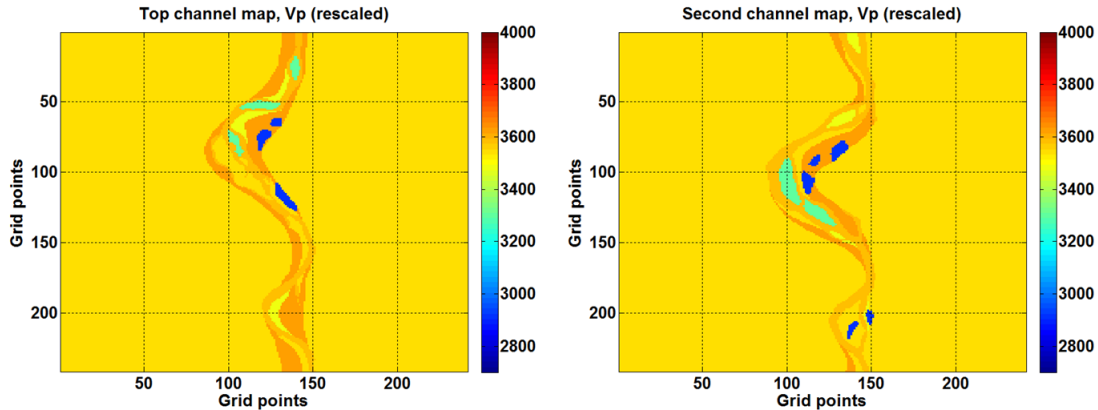
FIG. 3. Similar to Figure 1 except that the Vp values have been scaled by the factor 0.864 to reflect a change of the depth of burial from 1.5km to 1.0km.
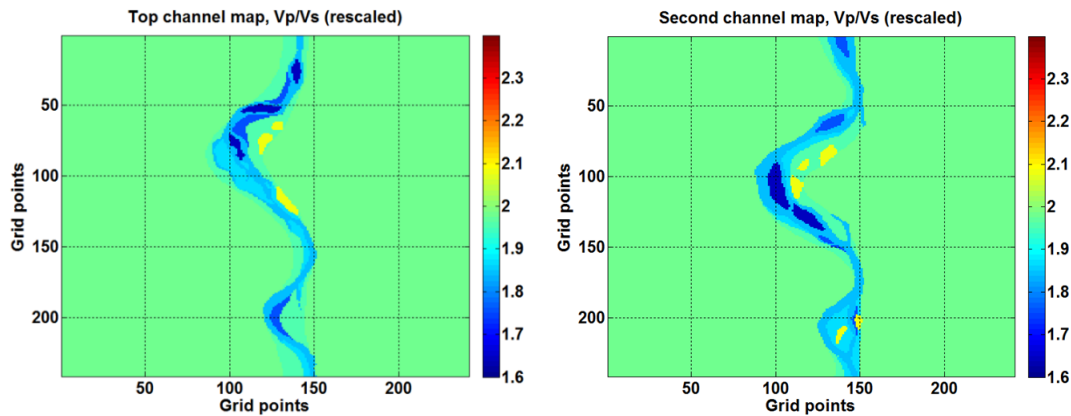
FIG. 4. Similar to Figure 3 except that the value of Vp/Vs is shown.

Kriging the 3D Volume

Initial planning called for a fundamental volume cell size of 10 meters so the 241x241 digitization grid represents an area of approximately 2.4km squared. Eventually the final model uses a horizontal grid of 11.56m and a vertical grid of 10m giving a final aperture of 2.774km squared. It was desired that the total channel system be at least 100m thick and, given 5 digitized maps, it was decided to interpolate two more maps between each of the 5 original, giving a total of 13 maps and a channel package thickness of 120m. The interpolation was accomplished by a 3D kriging process. The same kriging process was used to introduce material gradients within the polygons of the original maps. Kriging is a geostatistical spatial interpolation process that is often used to predict a regular grid of data from an irregular set of samples. To accommodate the kriging process, the original maps were sampled at between 200 and 300 locations on each map. Each map had unique sample locations with most samples being within the channel system but care was taken to also sample the surrounding region.

So, for example, let the first map be at depth z=0 and the second at depth z=30, and let theses maps be sampled at 200-300 irregularly positioned points. It is then desired to predict regularly sampled maps at z=0,10,20,30 from the irregular "data" points at the two bounding depths. Each predicted point is a linear combination of the data points and the linear weights come from the inversion of a covariance matrix that describes the spatial correlations between the data points themselves. For each predicated point, the inverted covariance matrix is multiplied into a covariance vector describing the correlations between the data and the prediction point. The spatial correlations were imposed using a correlation function based on the common 'spherical' variogram model.

Kriging was done using the Matlab program 'polykrig3D', which was written specifically for this project. It is designed to have an awareness of the polygons in the map slices and controls point-to-point correlations, based on the idea that they are more likely to be similar if located within the same polygon, and less likely to be similar if they are located in different polygons. Correlation is controlled through the definition of variogram 'ranges' which define the separation distance at which two points become uncorrelated, in polykrig3D the ranges are a pair of numbers assigned in each of the x, y, and z directions. Of the two numbers, the first defines the correlation of two points within

the same polygon, and the second defines the correlation of two points in separate polygons. Generally, much larger ranges were used for points in the same polygon than for those in different polygons. As this model involved a channel, it was initially thought that the ranges would be significantly different in the x and y direction, as the river flowed in a nearly constant-x (North to South) direction through the map area. How different the ranges should be , exactly, was unknown. As for the z-direction ranges, the only definite fact was that the 'same polygon' value had to extend over the spacing of two maps so that any correlation at all between the two would be incorporated into the model. For instance, with the genuine maps spaced every 30m and maps being kriged every 10m between them, the z range value for points correlated within the same polygon needed to be at least 20m. Ultimately, much testing was done with the range values to create the final models.

The spatial variability of the final model was further increased by imposing random fluctuations on the data points prior to the kriging process. In order for the channel to best reflect the variance found in sands within a river, it was necessary to allow randomness and variability to play a role within each single polygon. Although points within each single polygon are more likely to be similar, there is still some degree to which natural variations will occur. Due to the polygon's location in the channel system, it may be predisposed to a larger degree of randomness than another. For example, areas along the river which experience more variant water levels (like floodplains, terraces, or nearby ponds) will undergo discontinuous periods of sedimentation, and certain times where coarser materials can be deposited. We therefore assigned a particular variance to each lithology type.

Figure 5 shows how the maps of Figure 3 have changed after the sampling, incorporation of random fluctuations, and kriging. After considerable experimentation, the final kriging ranges used were isotropic in (x,y) although different in z. The rounded features evident in the region outside the channel indicate where sample points were taken in this area and are essentially an artefact of the process. Careful comparison of Figures 5 and 3 shows that the polygonal regions now have internal gradients and blurred boundaries. Figure 7 shows enlargements to facilitate this comparison. Figure 6 shows the two maps created between the maps of Figure 5 by the kriging process. In each one, both channels can be discerned but the closer one is more distinct.
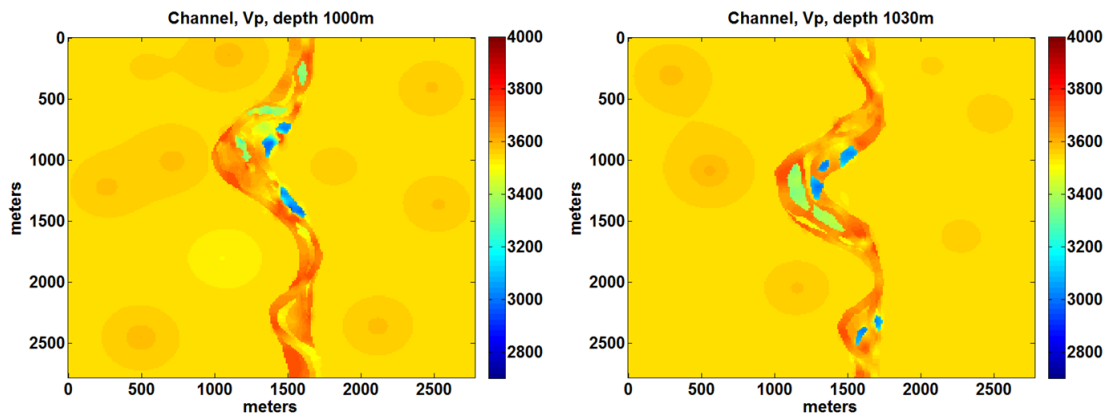
FIG. 5. The same maps of Figure 3 are shown after process of sampling, imposition of random fluctuations, and kriging. Note also the presence of physical distance scales.
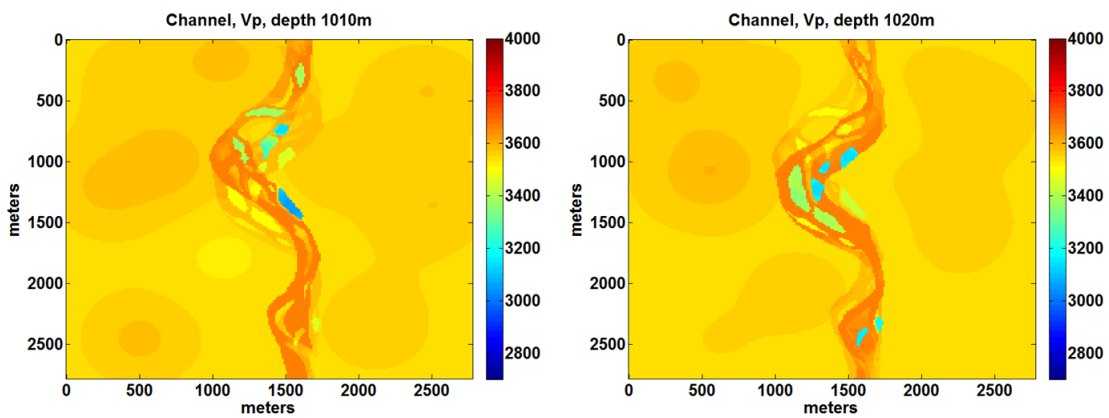
FIG. 6. The two maps between those of Figure 5 as predicted by the 3D kriging process described in the text.
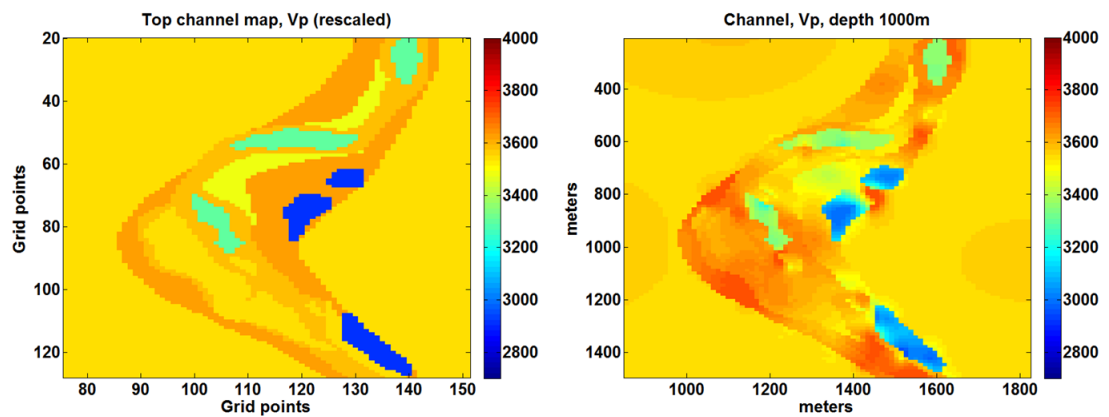
FIG. 7. Detailed comparison of the left-hand maps of Figure 3 (left) and Figure 5 (right). It is apparent that the polygonal bodies (left) have internal gradients and blurred boundaries after kriging (right).

Views of the Present Model

Figures 8, 9, and 10 show the complete channel sequence as finally created. Figure 8 displays the values of Vp, Figure 9 shows the ratio Vp/Vs, and Figure 10 shows the

density. As mentioned previously, prospective sand bodies are taken to be those with very low values of Vp/Vs.
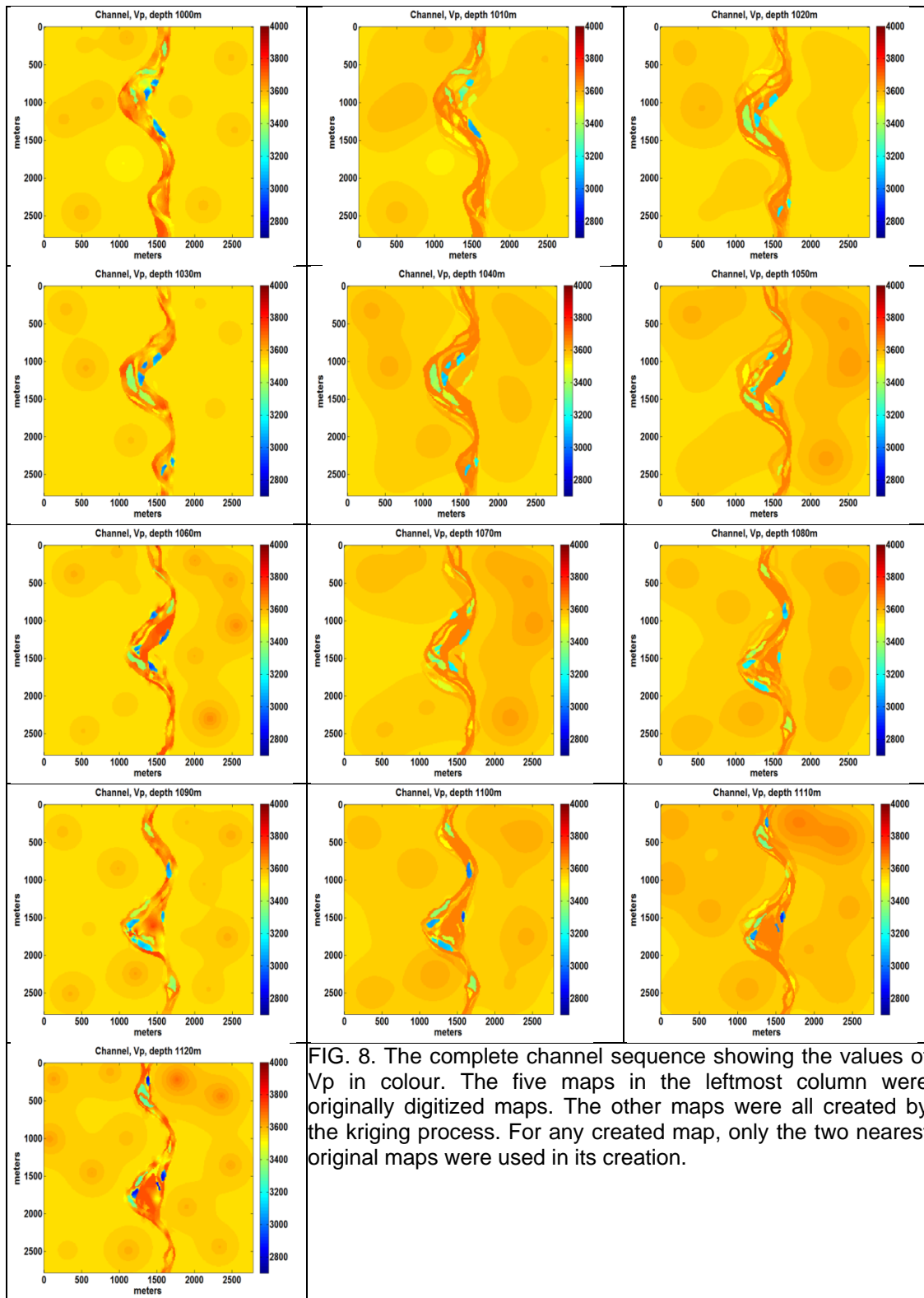
FIG. 8. The complete channel sequence showing the values of Vp in colour. The five maps in the leftmost column were originally digitized maps. The other maps were all created by the kriging process. For any created map, only the two nearest original maps were used in its creation.
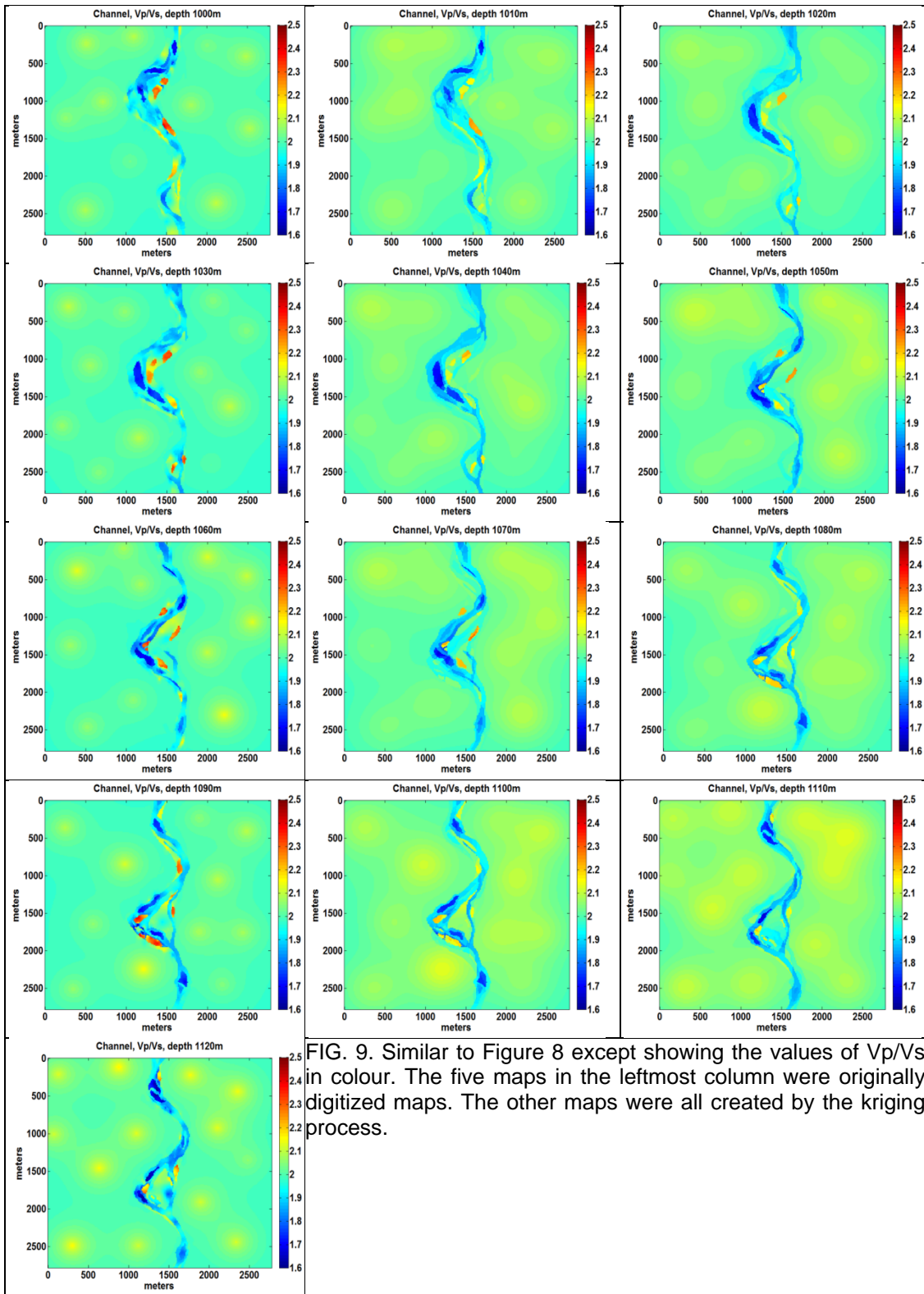
FIG. 9. Similar to Figure 8 except showing the values of Vp/Vs in colour. The five maps in the leftmost column were originally digitized maps. The other maps were all created by the kriging process.
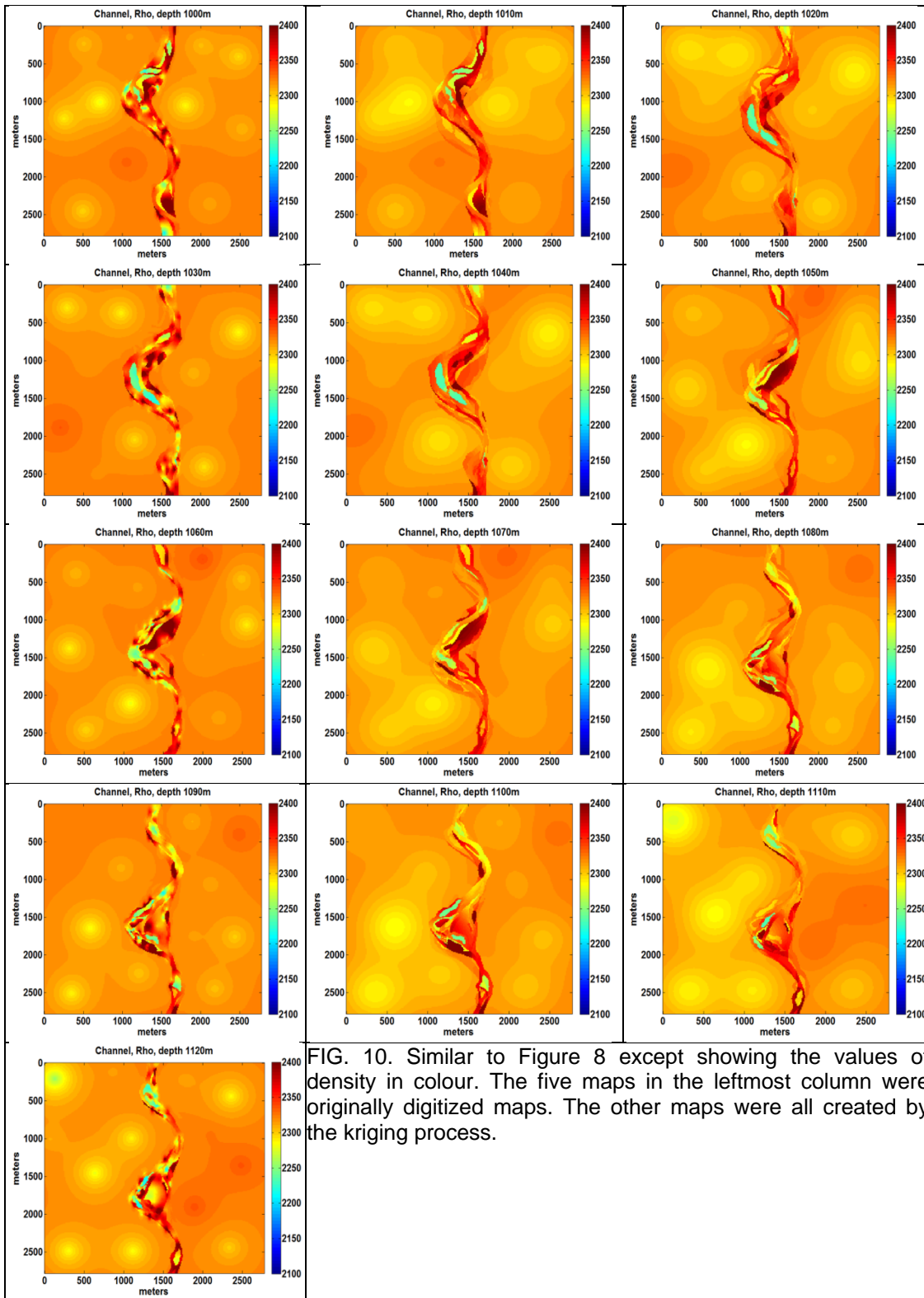
FIG. 10. Similar to Figure 8 except showing the values of density in colour. The five maps in the leftmost column were originally digitized maps. The other maps were all created by the kriging process.

The final model with overburden is illustrated by the profiles shown in Figures 11, 12, and 13 which show Vp. Vs. and density respectively. The "overburden" refers to the

curves shown in Figure 2 which describe the medium both above and below the channel sequence. The channel interval itself extends from 1000 to 1120m and "basement" begins at 1500m.
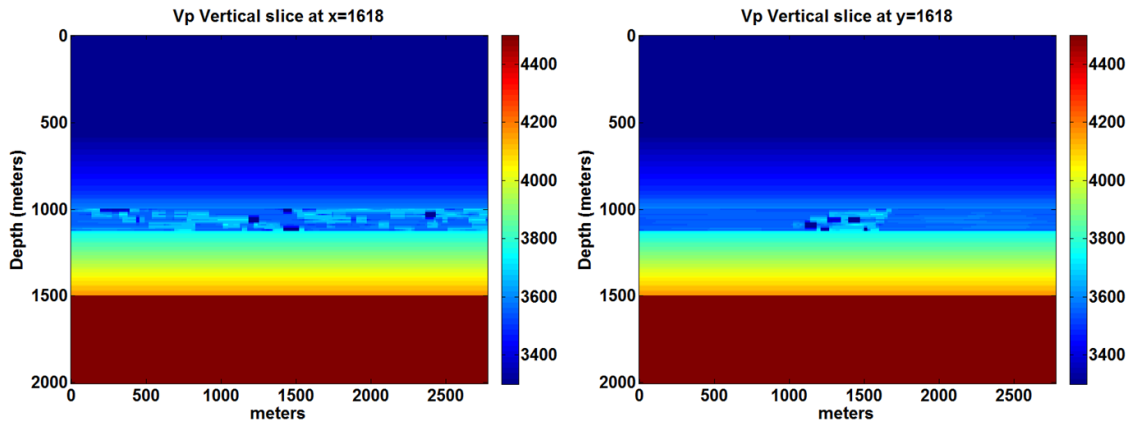
FIG. 11. Vertical cross sections through the final 3D model parallel to the channel at the central x coordinate (left) and orthogonal to the channel at the central y coordinate (right). Colour coding shows the value of Vp.
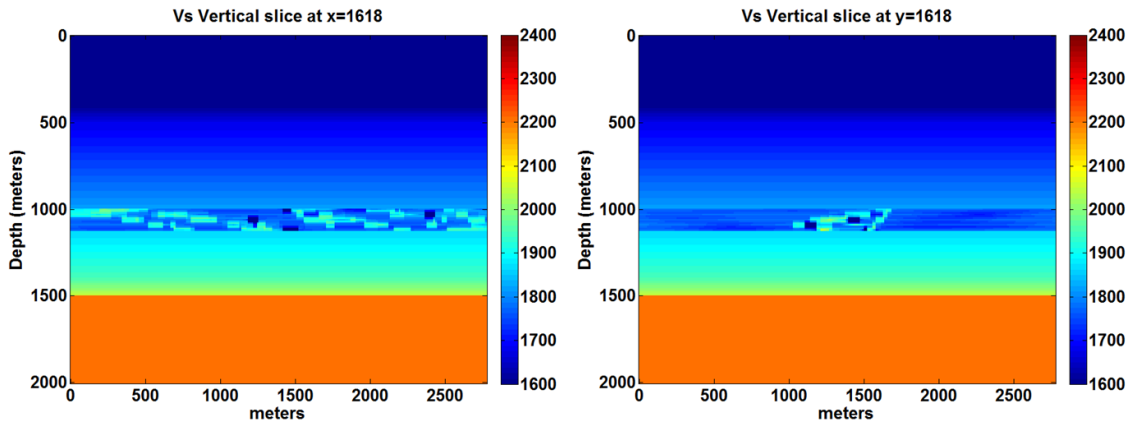
FIG. 12. Similar to Figure 11 except that colour coding shows the value of Vs.
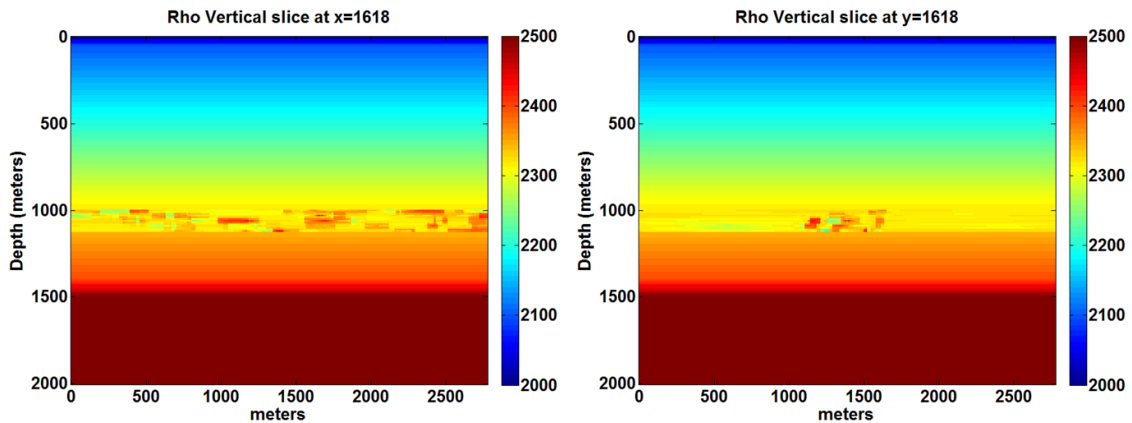
FIG. 13. Similar to Figure 11 except that colour coding shows the value of density.

Reef Model

We have also begun construction of a reef model based loosely on the Rainbow "A" structure. The process of creating the reef model was essentially similar to that used for the channel. As before 5 maps representing different depth slices through the structure were hand-drawn and digitized and then lithologies were assigned to polygonal regions. As before, these maps representing polygonal regions with homogeneous properties were then sampled, subjected to random variation, and then 3D kriging was used to interpolate between maps.
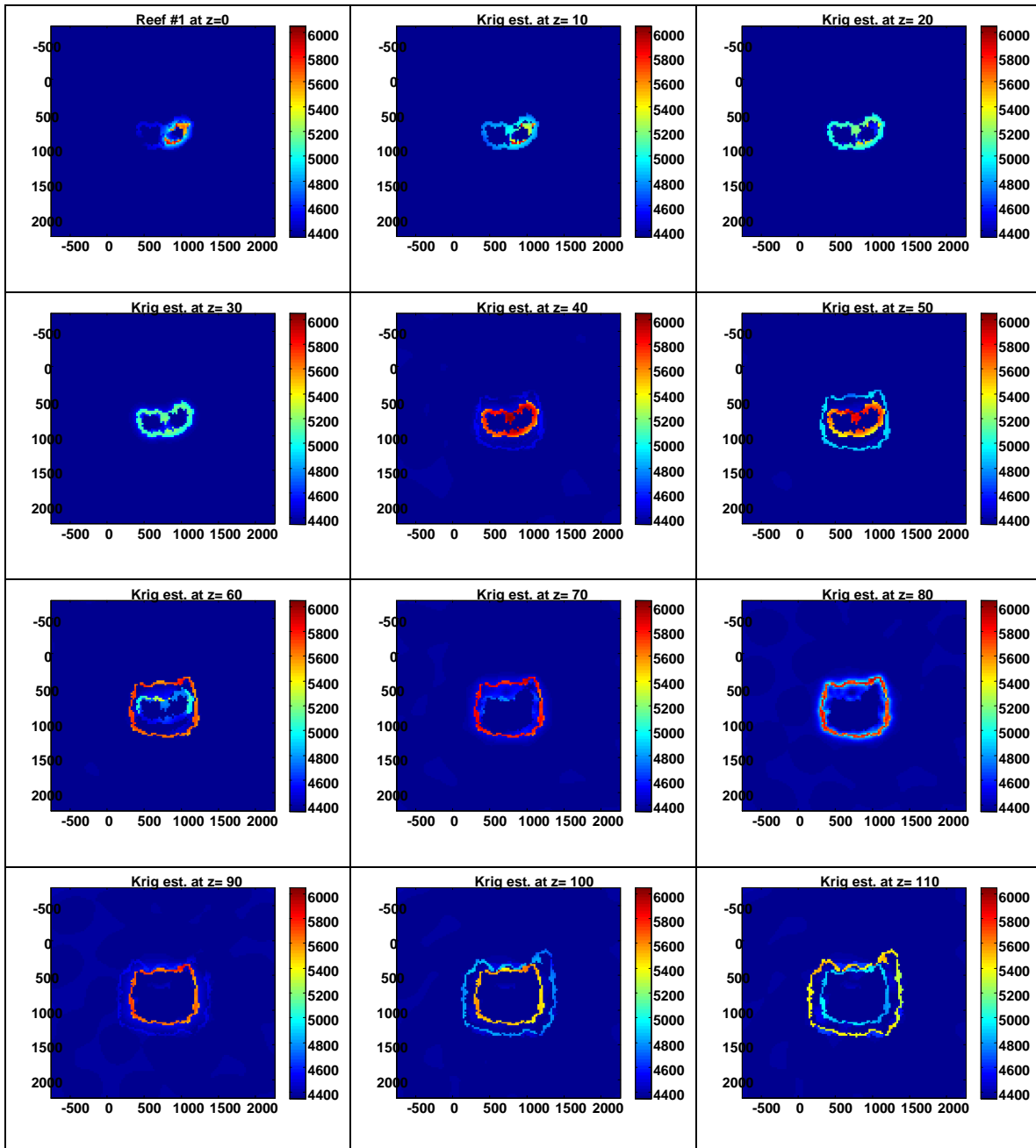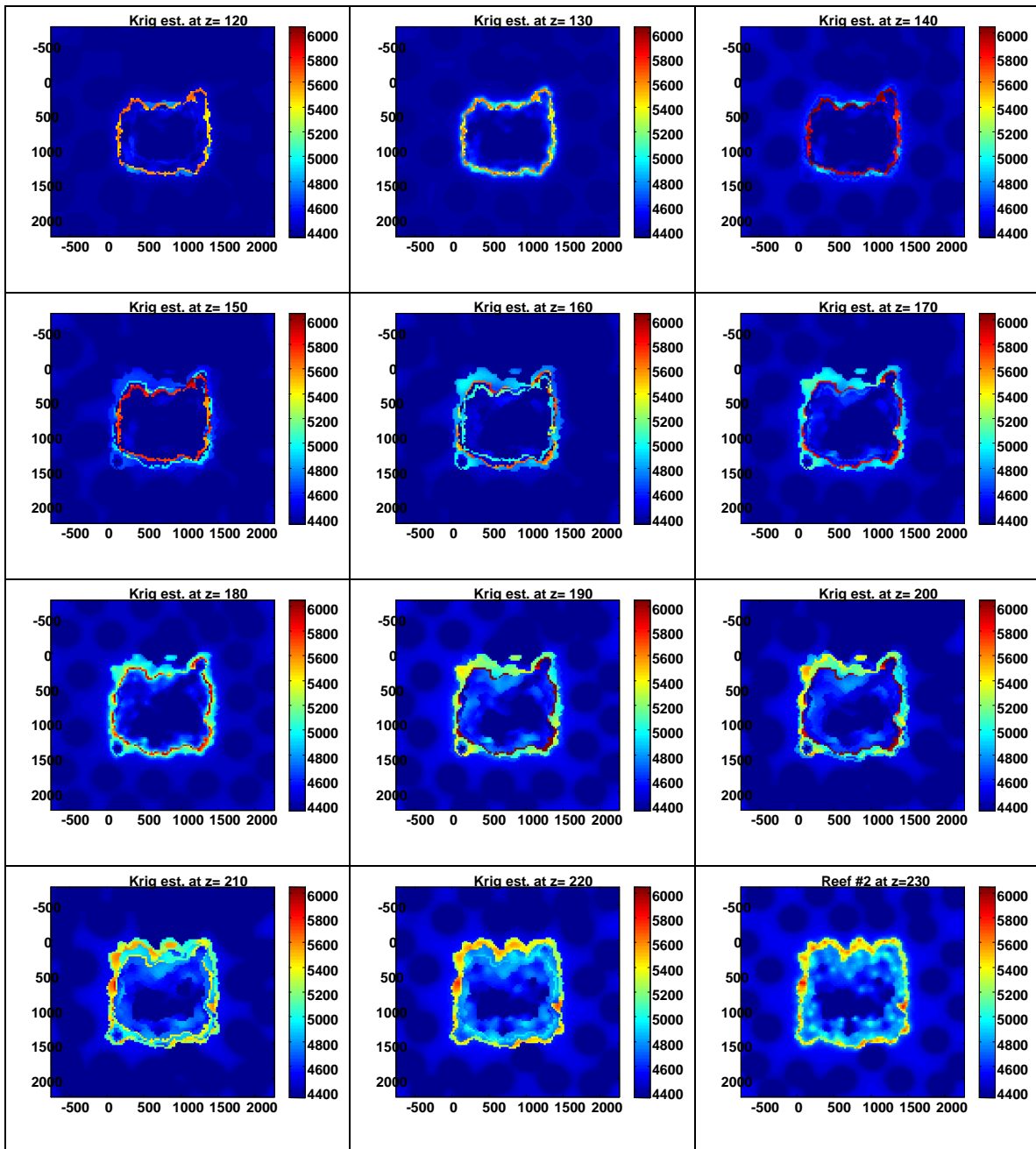
FIG. 14. A series of images representing Vp values at constant depth slices through the reef. Beginning with the upper left figure which represents the cap rock, slices descend through the reef at 10m intervals. This sequence of images in considered preliminary in that it is apparent that more points needed to be chosen in the regional area outside the reef to reduce the circular artifacts.
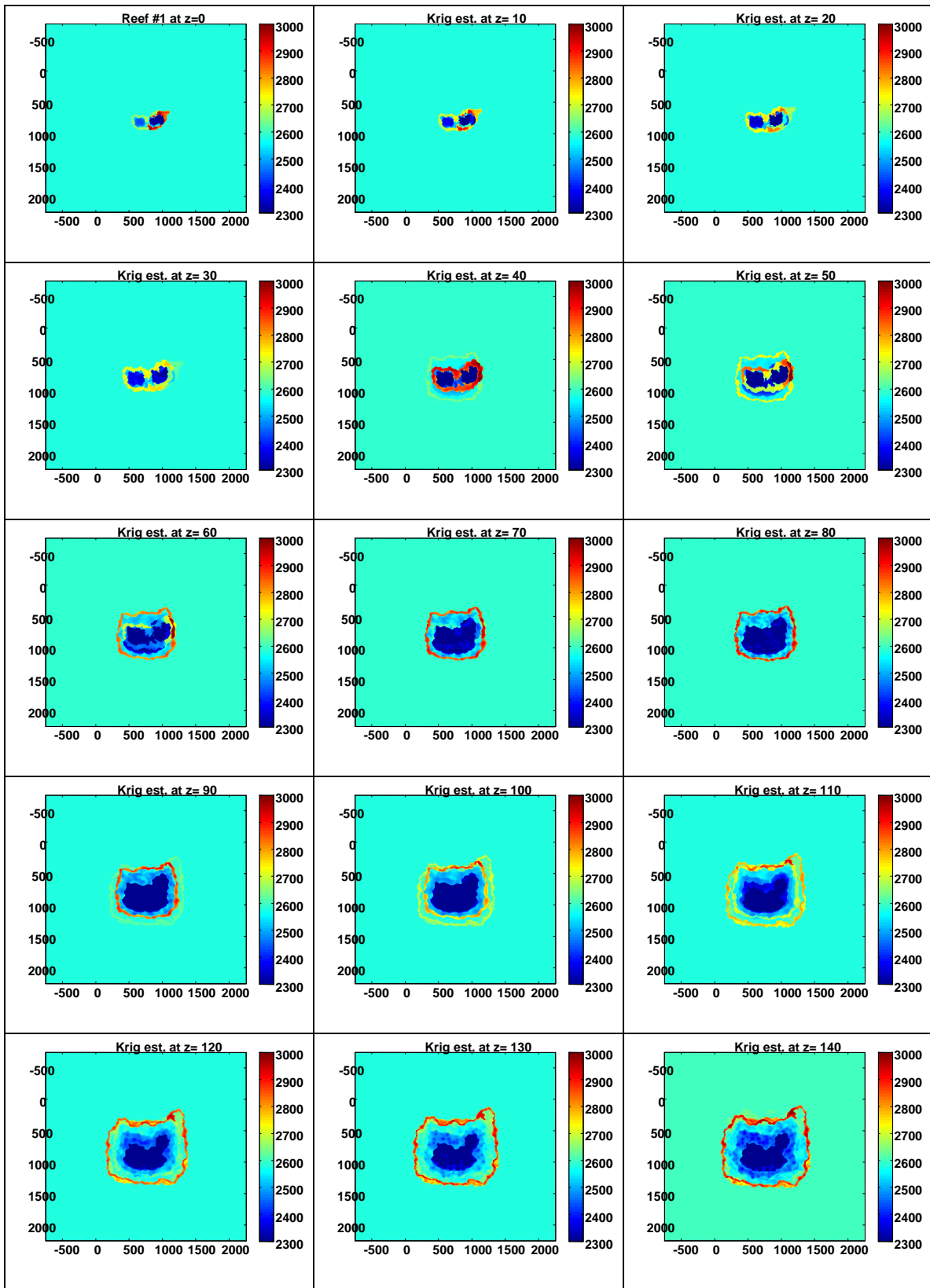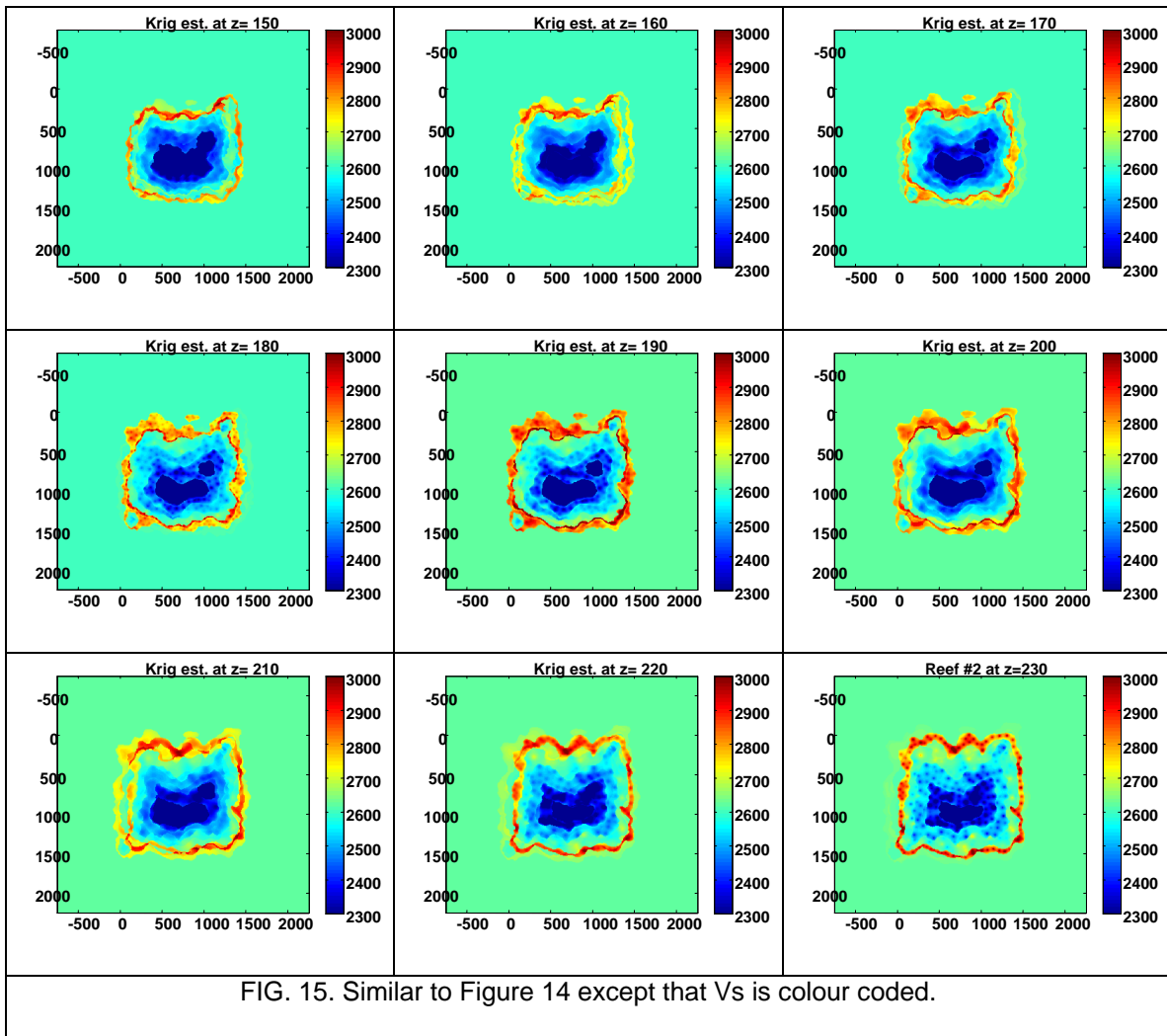
FIG. 15. Similar to Figure 14 except that Vs is colour coded.
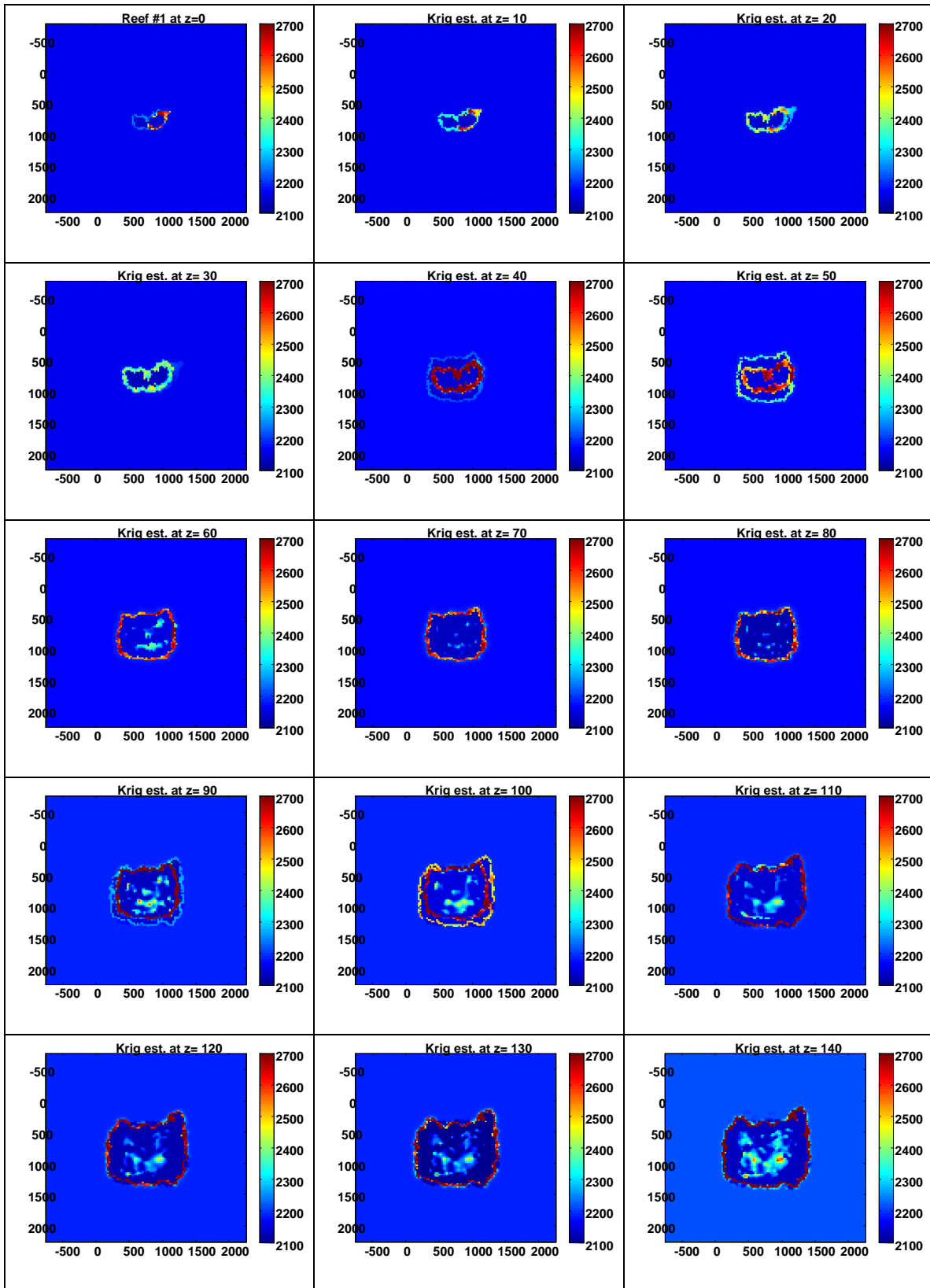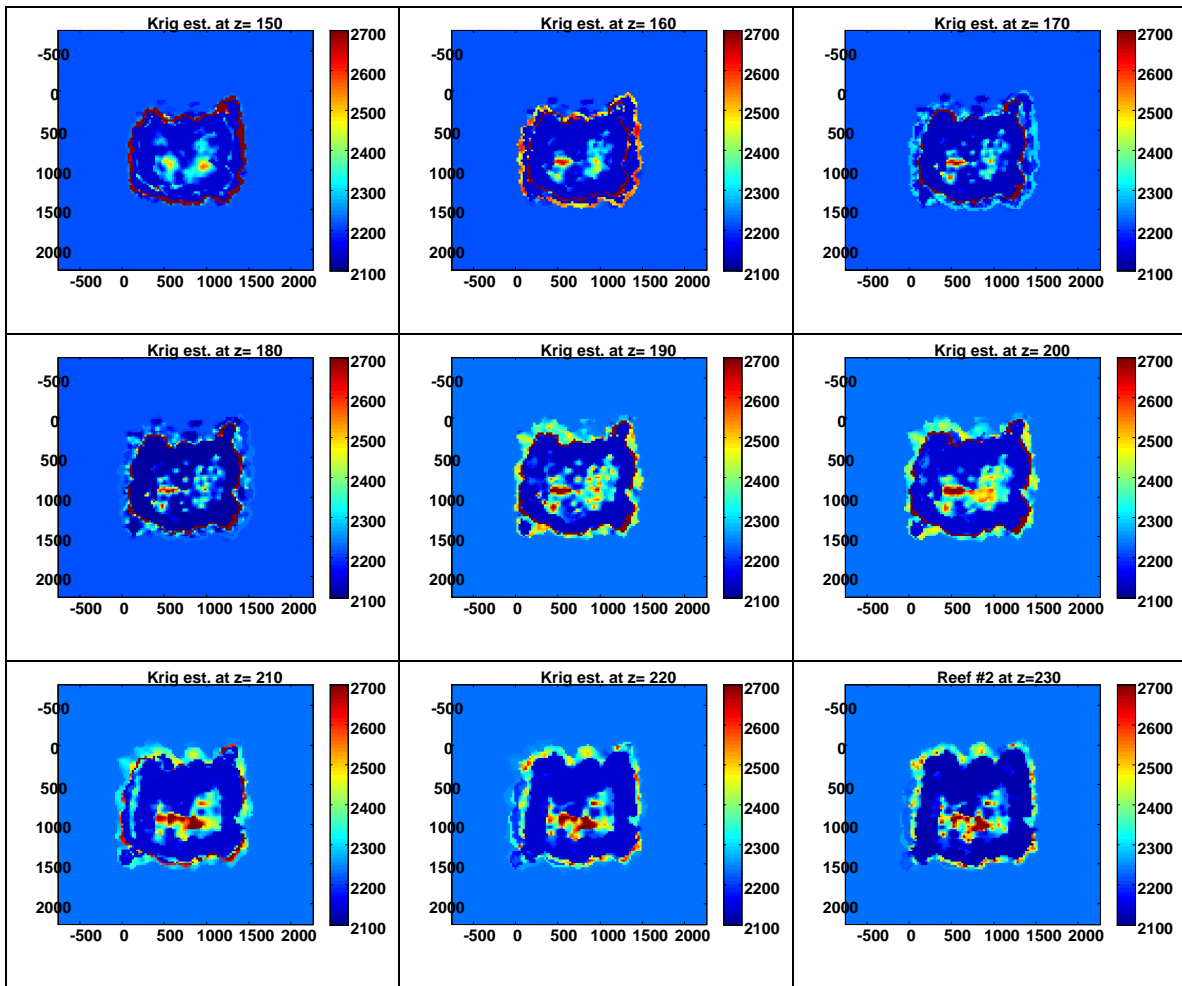
FIG. 16. Similar to Figure 14 except that density is colour coded.
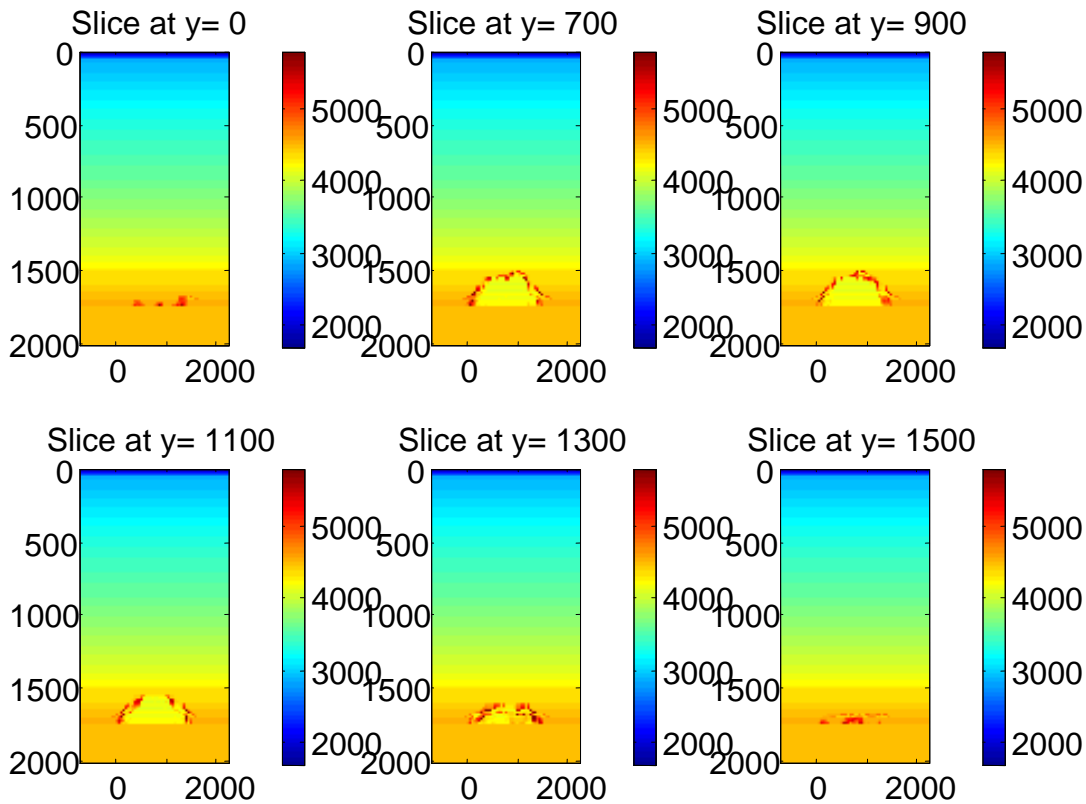
FIG. 17. A series of vertical cross sections through the reef model with the overburden attached. Colour coding indicates Vp.

SEISMIC WAVE SIMULATIONS

Simulating seismic shot records in a model as complex as those described here requires sophisticated software. We show here results using the 3D modelling software Tiger, by SINTEF Petroleum Research[2] of Trondheim, Norway. This application is a very full-featured and technically sophisticated 3D finite difference modelling program for acoustic, elastic or visco-elastic media with or without anisotropy. In the present context, we used only the acoustic and isotropic elastic capabilities. Tiger uses 8th order spatial differencing and, presumably, second order in time. The application is parallel-aware and able to distribute the computation of individual shot records across a Linux cluster. (A single shot record is not run in parallel.) CREWES has acquired a 1-year, single-seat license for Tiger and we are presently evaluating it. We also show here results from our Rayleigh-Sommerfeld algorithm that has been modified to include P-P AVO. This method is capable of a much higher frequency response than finite-difference but it does not compute the complete wavefield. Only specifically designated reflections are computed.

Tiger is essentially a batch unix program with a rudimentary GUI front-end that builds the necessary job files. The documentation is minimal and a considerable amount of technical knowledge is required to install and run the program. This is understandable as the software is only recently developed and CREWES is one of the first users and we are

---

[2] *www.**sintef**.no/upload/Petroleumsforskning/Brosjyrer/**TIGER**.pdf*

definitely the first academic user. Running Tiger requires preparation of 3D volumes for each elastic parameter as disk files in a format that Tiger understands. Formats include SEGY, SU, and DIR. Since we developed our model in Matlab, it was a fairly simple matter to write a Matlab function that outputs our model in SU format. In addition to the isotropic elastic parameters (P and S velocities and density) which we supplied, Tiger can also accept 3D volumes of Thomsen anisotropy parameters, polarization and azimuthal angles, and P and S quality factors. We have not yet tested these options. Once datasets have been loaded, then Tiger requires a wavelet, either created or imported, and a source/receiver geometry specification. All ordinary acquisition geometries can be easily simulated. The final step is to specify and quality-control the parameters of the simulation. An automatic stability and dispersion analysis can be run to help choose optimal parameters. Boundary reflections are suppressed by the perfectly matched layer (PML) technique.
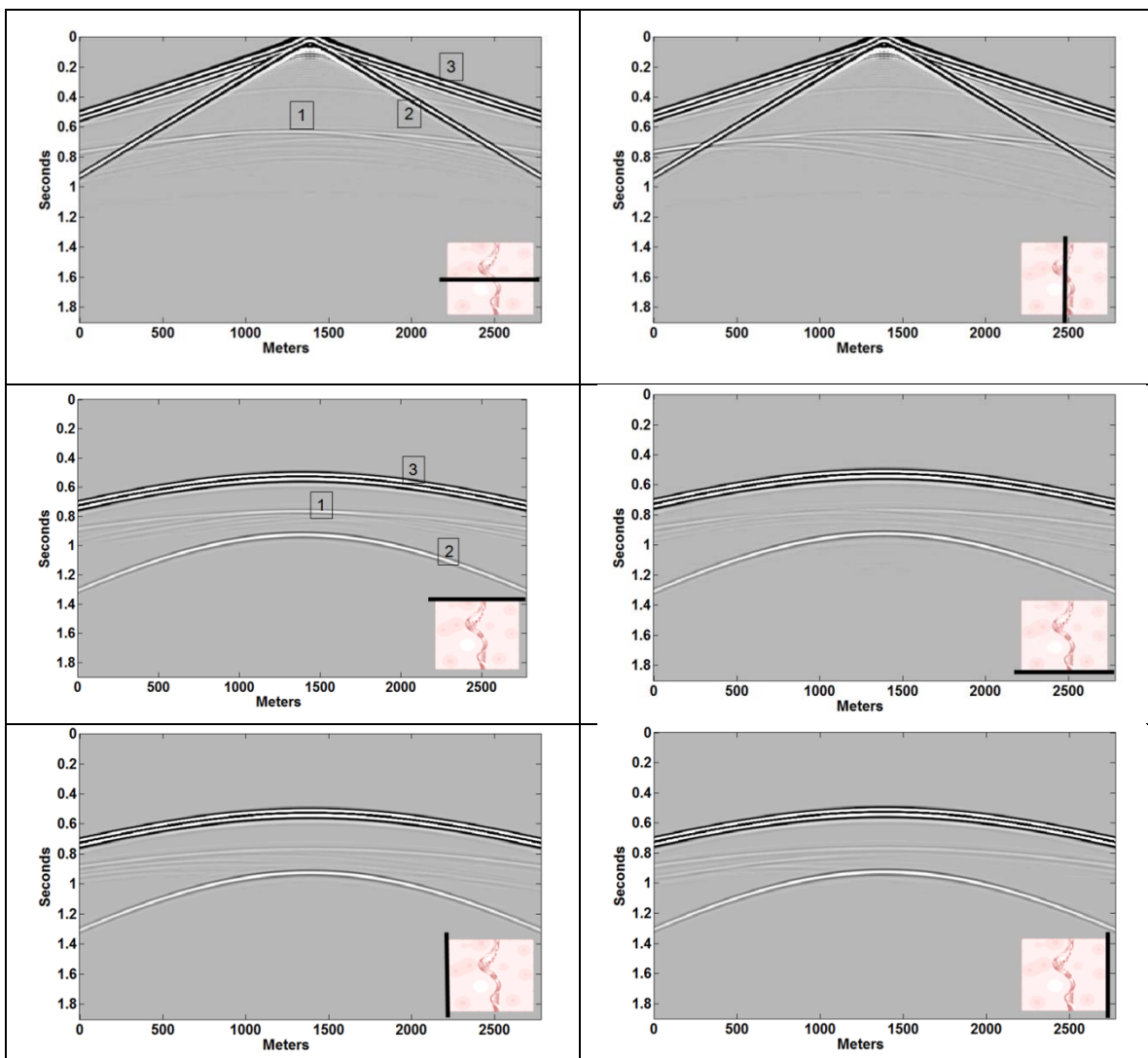
FIG. 18. A series of 2D views through a 3D shot record computed by Tiger when running in an acoustic mode. The shot location was in the centre of the model and the location of the receiver line for each profile is indicated by the black line on the small insert map. Labelled events are (1) the channel sequence, (2) the direct p-wave, and (3) a shallow reflection. Each profile shows the vertical component of particle displacement.

Figure 18 shows a series of vertical profiles through a single 3D shot computed by Tiger when running in an acoustic mode using only the Vp and density channel models. Thus there are no shear waves in this simulation. The channel sequence is evident as a complex series of events labelled (1) in the Figure. The wavelet used is a 30 Hz, zero phase Ricker. These profiles are displayed without amplitude adjustment but with various clip levels to make visible the significant events. Figure 19 is a similar series of vertical profiles computed in an identical fashion to those of the previous figure except that an elastic solution was chosen. Among the notable differences between the acoustic and elastic cases are the multiple surface modes in the latter (the events marked 2) and the basement reflection (4) which is not visible in the acoustic case. The reason for the absence of the basement reflection in the acoustic case is not presently known. Figure 20 shows a similar acoustic solution to that of Figure 18 except that only the topmost channel layer was included in the model; and the basement reflection is now visible. It is conjectured that the downgoing acoustic primary wave is strongly attenuated by multiple scattering through the complex channel sequence while, for reasons not evident, the elastic P-wave is not so strongly affected.
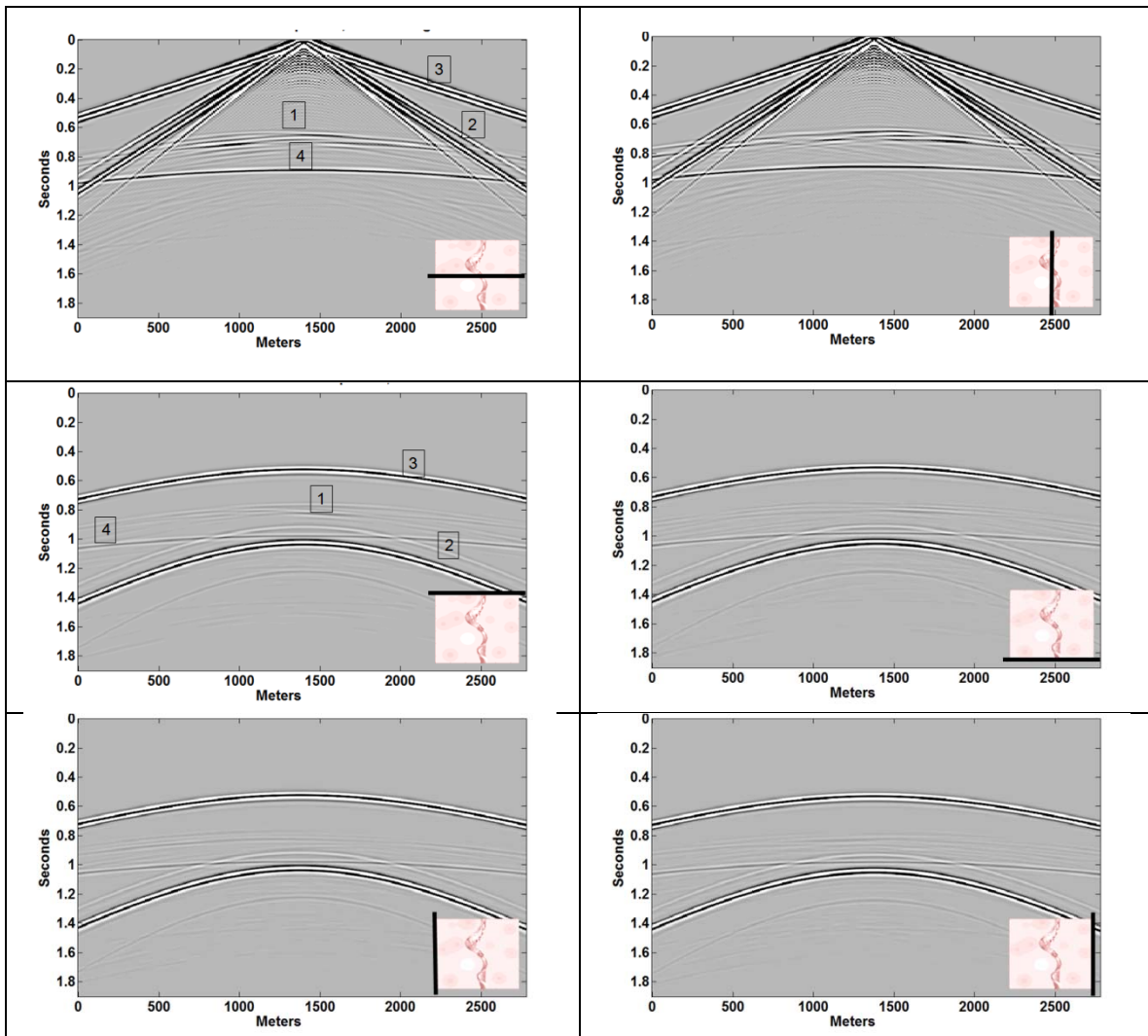
FIG 19. Similar to Figure 18 except that the solution is now elastic. Labelled events 1-3 are the same as the previous figure: (1) the channel sequence, (2) the direct p-wave, and (3) a shallow

reflection. Event 4 was not seen previously and is the basement reflection from the impedance increase at 1500m (see Figure 2).
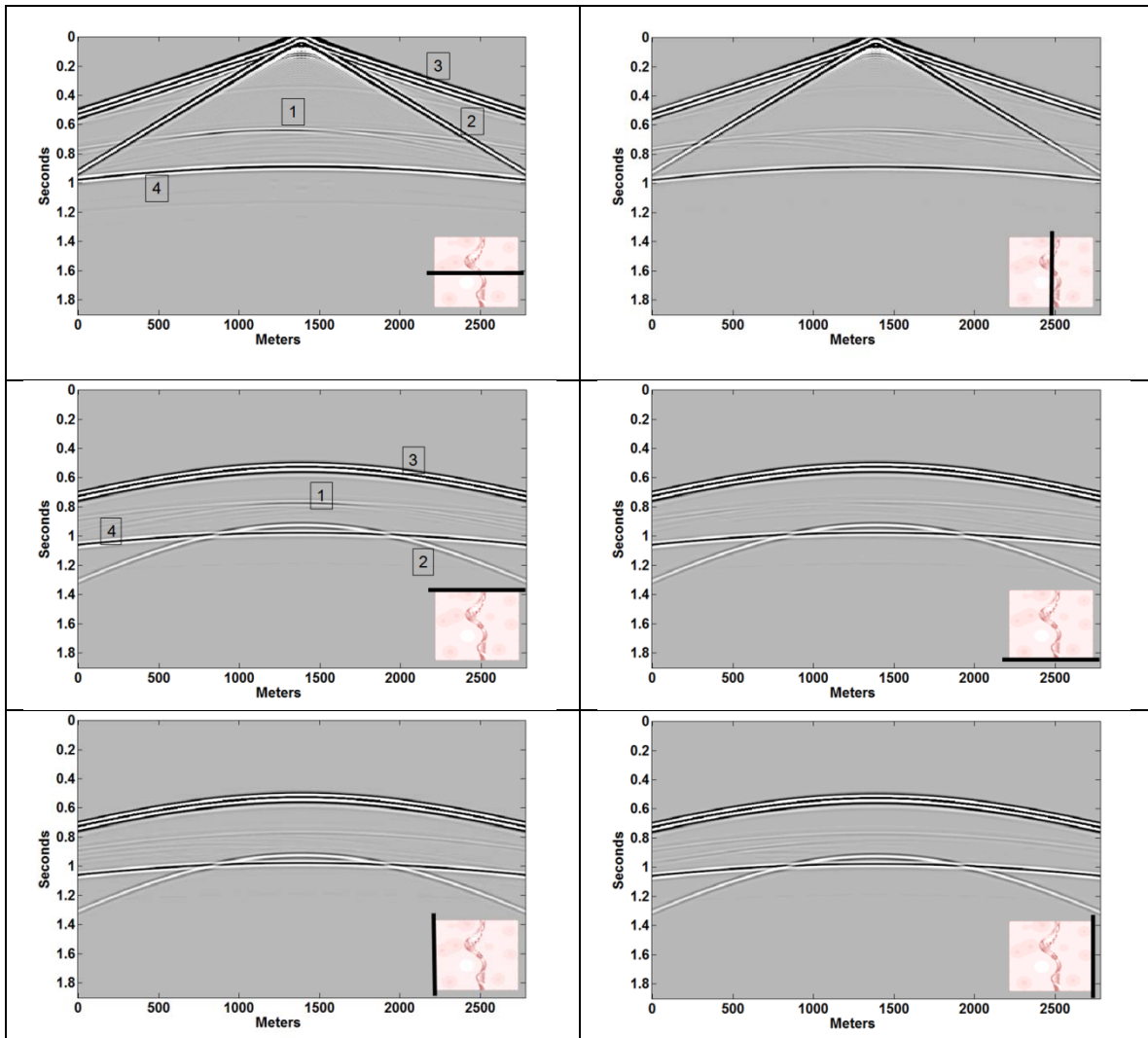
FIG. 20. Similar to Figure 18 except that only the uppermost channel level was included in the model, making the channel thickness only 10m. Notice the appearance of event 4, which is the reflection from the basement.

Figure 21 shows the result of the Rayleigh-Sommerfeld algorithm (Margrave and Cooper, 2007) on a model with a single channel level and another featureless reflector placed between the channel and the surface. This computation is described in more detail in Cooper et al. (2008). The Rayleigh-Sommerfeld computation has about twice the bandwidth of the finite difference and was computed in about 5% of the time. However, our Rayleigh-Sommerfeld algorithm does not compute surface waves and propagates the waves only through the background medium. The latter restriction is not essential and should be surmounted in the coming year.
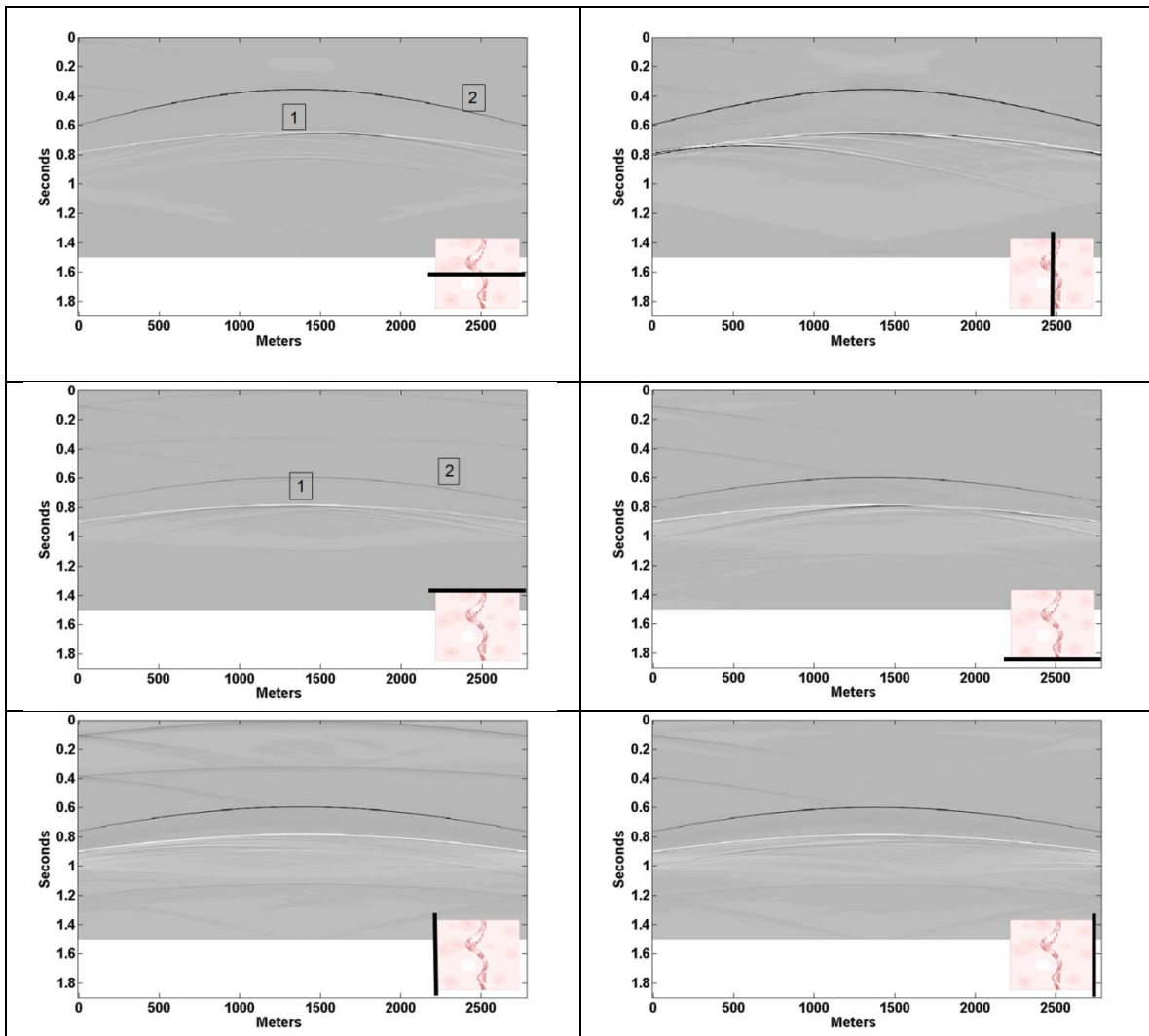
FIG. 21. A Rayleigh-Sommerfeld solution for the case of only a single channel level as in Figure 20. Event 1 is the channel reflection while event 2 is a single featureless reflector not included in the previous simulations. The frequency bandwidth is much broader than in the finite-difference simulations. Also note the lack of surface waves.

Figure 22 shows time slices through the four different solutions shown in Figures 18, 19, 20, and 21. While broadly similar, the higher spatial resolution of the Rayleigh-Sommerfeld solution is immediately apparent. Also additional surface waves of the elastic solution are eveident.
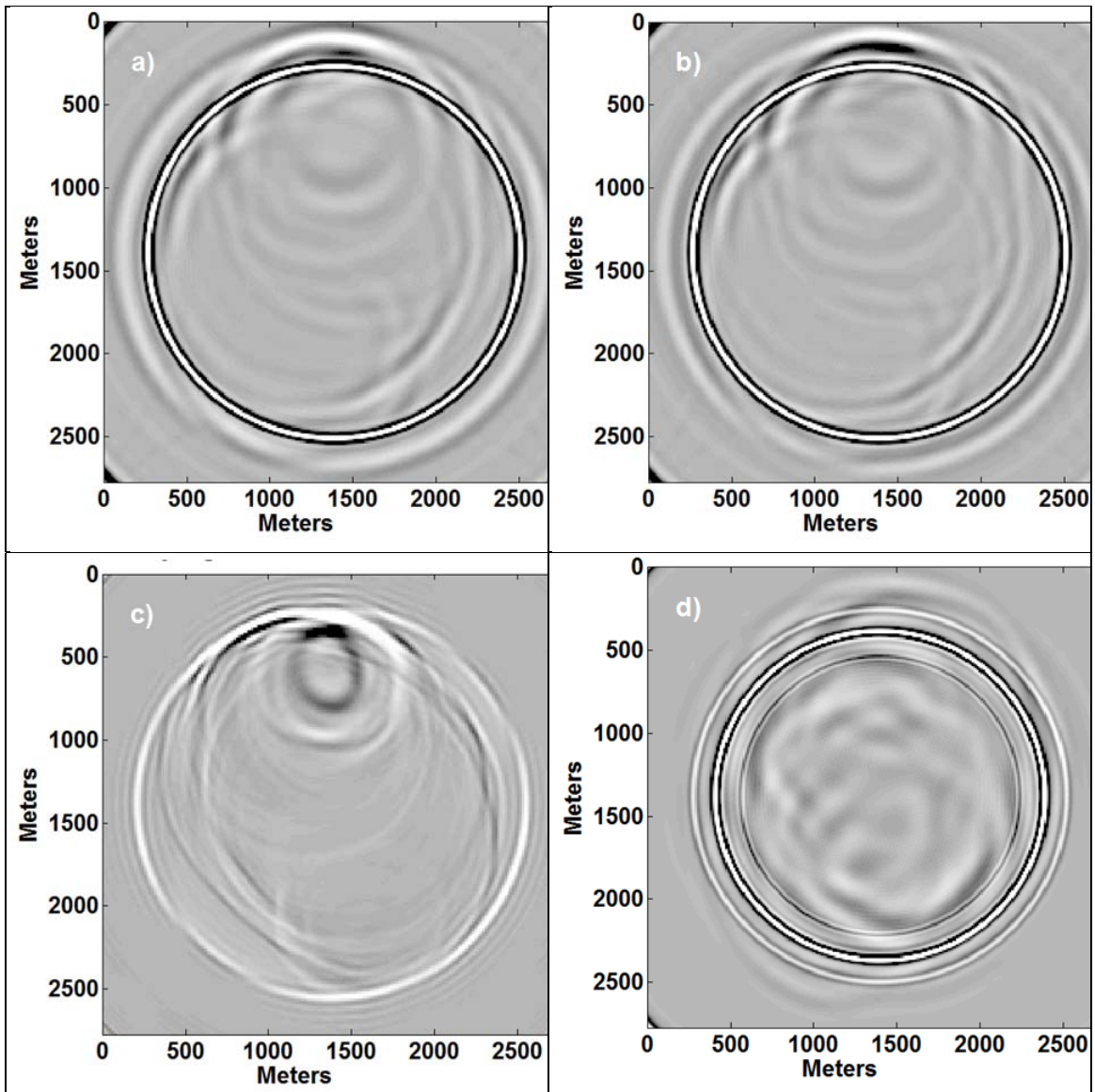
FIG. 22. Time slices at 0.75 seconds through the solutions of the previous four figures. (a) is the acoustic solution for the full channel model, (b) is the acoustic solution for a single thin channel layer, (c) is the Rayleigh-Sommerfeld solution, and (d) is the full elastic solution.

DISCUSSION AND CONCLUSIONS

We have begun the process of creating realistic models of the spatial distribution of the isotropic elastic parameters for Canadian stratigraphic targets. In particular, we have modelled a buried channel sequence patterned after the modern Bow River and a pinnacle reef patterned after the Rainbow "A" structure. Our channel model is the more mature of the two. Both models were built by first constructing geologically plausible maps at a small number of depth levels within the envisioned structure. Then a specially constructed 3D kriging process was used to both interpolate between these maps and to introduce material gradients within the maps. The resulting channel structure contains 13 defined levels and represents a 120m depth sequence. The overburden and underlying sequence are horizontally stratified and defined from typical well logs. The final channel model has the structure at 1km depth within a 3D volume that is 2.7km- by 2.7 km in

areal extent and 2.0 km in depth. The resulting digital volume is 241 by 241 by 201 points.

Our models are not intended to represent specific structures but rather to give realistic seismograms to test the ability of our imaging and inversion techniques. We are in the process of creating the elastic seismic records predicted by our models. We have illustrated several such records here as created by the commercially available Tiger program by SINTEF Petroleum Research[3] of Trondheim, Norway, and by our own research code using the Rayleigh-Sommerfeld approximation. The results are pleasingly complex and realistic. We anticipate that full 3D datasets corresponding to realistic acquisition geometries will be available for release to sponsors in 2009. Furthermore, we will use these models to study the seismic footprint and to evaluate our imaging and migration methods. We invite suggestions for alternative model parameters or for completely new models. A major goal in the coming year will be the creation of models involving VTI and HTI anisotropies and we invite suggestions for these.

ACKNOWLEDGEMENTS

REFERENCES

Cooper, J. K., Margrave, G. F., and Maweu, J, 2008, Rayleigh-Sommerfeld modelling with AVO, CREWES Research Report, **20**.

Hills, L., 2002, The last 20000 years in the Calgary area: in Breaking Ground, Creating a Greener Healthier City, Conference Proceedings.

Osborn, G. D., and R. Rajewicz, 1998, Urban Geology of Calgary, *in* P. F. Karrow and O. L. White, eds., Urban Geology of Canadian Cities: Geological Association of Canada Special Paper 42, 93-115.

Margrave, G. F., and Cooper, J. K., 2007, Seismic modelling in 3D for migration testing, CREWES Research Report,**19**.

---

[3] *www.**sintef**.no/upload/Petroleumsforskning/Brosjyrer/**TIGER**.pdf*